Components of the Plasma Membrane of Growing Axons. II. Diffusion of Membrane Protein Complexes

ROCHELLE K. SMALL, MARTIN BLANK, RICHARD GHEZ, and KARL H. PFENNINGER
Department of Anatomy and Cell Biology and Department of Physiology, College of Physicians and Surgeons, Columbia University, New York 10032; and Thomas J. Watson Research Center, International Business Machines Corporation, Yorktown Heights, New York 10598. Dr. Small's present address is Department of Pathology (Immunology), Yale University School of Medicine, New Haven, Connecticut 06510.

ABSTRACT Intramembrane particles (IMPs) of the plasmalemma of mature, synapsing neurons are evenly distributed along the axon shaft. In contrast, IMPs of growing olfactory axons form density gradients: IMP density decreases with increasing distance from the perikarya, with a slope that depends upon IMP size (Small, R., and K. H. Pfenninger, 1984, *J. Cell Biol.*, 98: 1422–1433). These IMP density gradients resemble Gaussian tails, but they are much more accurately described by the equations formulated for diffusion in a system with a moving boundary (a Stefan Problem), using constants that are dependent upon IMP size. The resulting model predicts a shallow, nearly linear IMP density profile at early stages of growth. Later, this profile becomes gradually transformed into a steep nonlinear gradient as axon elongation proceeds. This prediction is borne out by the experimental evidence. The diffusion coefficients calculated from this model range from 0.5 to 1.8×10^{-7} cm^2/s for IMPs between 14.8 and 3.6 nm, respectively. These diffusion coefficients are linearly dependent upon the inverse IMP diameter in accordance with the Stokes-Einstein relationship. The measured viscosity is approximately 7 centipoise. Our findings indicate (*a*) that most IMPs in growing axons reach distal locations by lateral diffusion in the plasma membrane, (*b*) that IMPs—or complexes of integral membrane proteins—can diffuse at considerably higher rates than previously reported for iso-concentration systems, and (*c*) that the laws of diffusion determined for macroscopic systems are applicable to the submicroscopic membrane system.

The extension of an axon by the neuron involves rapid, vectorial expansion of the plasma membrane. This is largely achieved by the addition of packets of plasmalemmal precursor in the form of vesicles at the distal tip of the advancing axon (e.g., 29, 31). This precursor membrane contains few intramembrane particles (IMPs; 46), which are believed to be complexes of integral membrane proteins (e.g., 5, 25, 45). In the growing axon's plasma membrane, the profile of components as seen by freeze-fracture changes as a function of distance from the perikaryon (see our companion paper, reference 46). A similar distribution is also seen for saxitoxin binding sites, putative Na^+-channels (see our companion paper, reference 49). These observations suggest that IMPs—or complexes of integral membrane proteins—are inserted into the plasmalemma proximally, at the perikaryon, and diffuse laterally within the plane of the membrane to reach the distal neuritic shaft. In this paper, we describe an analysis of the IMP density data in terms of diffusion in a system that expands with time. The resulting model matches the measured values with a high degree of accuracy and, therefore, strongly supports the diffusion concept. Thus, the investigation of IMP distribution in the growing axon gives insight into diffusion processes in the plasma membrane over extended time periods and long distances and, in particular, in a chemical gradient, a nonequilibrium system. Thus, the growing axon offers a new perspective of lateral diffusion in biological membranes.

Biological Systems

The olfactory nerves of adult bullfrogs provide a homogenous source of long, unmyelinated axons, which have been examined segmentally at maturity and during growth. A well

THE JOURNAL OF CELL BIOLOGY · VOLUME 98 APRIL 1984 1434–1443

synchronized population of growing neurites has been obtained by experimentally lesioning the mature nerve. When olfactory axons are severed their perikarya degenerate, and neurons are formed *de novo* from epithelial stem cells (16). Growing nerves were examined 5 wk after lesion, at an early stage of their growth toward synaptic targets. If a 1-wk interval is assumed to be taken up by the degenerative and mitotic events that precede neuritic outgrowth, then the time of actual axon growth is ~4 wk. Because we do not know this time exactly we assume a duration of 28 ± 5 d for our calculations. The average length of the growing nerves, 9.66 ± 0.48 mm, suggests a growth rate of 0.35 mm/d or $4.0 \cdot 10^{-7}$ cm/s. The spatial distribution of IMPs in mature and growing neurons has been determined by analyzing freeze-fracture replicas of the perikaryon, identifed segments along the axonal shaft, and the growth cone. A detailed description of the methods used is provided in the preceding paper (46). The smallest IMP size class, designated 4 nm in the preceding paper, includes particles between 4.7 nm and the resolution limit of the method, ~2.5 nm. To obtain an accurate curve of diffusion coefficients vs. IMP size, these particles are plotted by their approximate average size, 3.6 nm.

Freeze-fracture electron micrographs of short neurite sprouts were obtained from rat superior cervical ganglion neurons that were mechanically dissociated, seeded into culture dishes and grown in vitro for 1 to 2 d. For comparison, explants of rat superior cervical ganglion were grown in culture for 4 d. The cultures were then fractured and processed according to the methods described elsewhere (30, 32).

RESULTS

Spatial Distribution of Particles in the Plasmalemma of Growing Neurons

The distribution of plasmalemmal IMPs of growing olfactory neurons has been described in detail in the first paper of this series (46) and can be summarized as follows: After 4 wk of growth, IMP densities of the perikarya are similar to those of mature neurons (2,600/μm^2 in growing vs. 2,750/μm^2 in mature neurons for P-face). Along the shaft, however, IMPs of growing neurons form steep density gradients—quite unlike the IMPs of mature axons, which occur at uniform density (900/μm^2). Total IMP density in the growing axon decreases from ~1,100/μm^2 in the proximal shaft to 350/μm^2 at the distal tip (P-face values). Moreover, when IMPs are assigned to classes according to their diameter (3.6 to 14.8 nm) the densities of the individual size classes also decrease along the neurite, and the slopes of the resulting gradients are dependent upon IMP size. However, it is important to note that perikaryal and growth cone plasmalemma are not part of these IMP density gradients.

As indicated in the first paper of this series (46), the IMPs's spatial distribution can be reasonably well fitted to a Gaussian tail, regardless of particle size: If N is the area density of IMPs in the axolemma, then

$$N = a \exp(- bx^2) + c, \qquad [1]$$

where x is the distance measured from the axon hillock and a, b, and c are constants that depend on particle size. The constant c was identified with the measured IMP density, N_v, in growth cone vesicles (i.e., plasmalemmal precursor vesicles). It was also observed that the constant b is proportional to IMP size. As shown in Fig. 1 (cf. Table I), a semilogarithmic plot of normalized IMP densities against the squared distance (normalized for different IMP sizes; bx^2) produces a single, approximately linear population of points ($r^2 = 0.9506$). This result suggests that, in the growing axon, the distribution of IMPs of all sizes is controlled by a common mechanism, and that this mechanism may be lateral diffusion within the plasmalemma. However, if diffusion is responsible for IMP distribution along the growing axon, our mathematical model must take into account that, from the onset of axon formation, diffusion of IMPs and axon elongation occur concomitantly. The Gaussian function, Eq. 1, disregards this property of our biological system and, therefore, is an approximation at best. We now formulate a model that satisfies the conditions of lateral diffusion in an elongating axon.

The Diffusion Model

The underlying problem is one of diffusion in a system with a moving boundary, a so-called Stefan Problem (37). Such phenomena often occur in physicochemical processes, notably during phase changes. Let L be the axon's length at time t. Then the one-dimensional diffusion equation for the density $N(x,t)$ reads

$$\frac{\delta N}{\delta t} = D\frac{\delta^2 N}{\delta x^2}, \qquad [2]$$

in the expanding region $0 < x < L(t)$. This equation simply states that diffusion is the only driving force along the membrane, that the diffusion coefficient D is assumed a constant (cf. below, however), and that IMPs are neither created nor destroyed during their diffusive motion.

A first boundary conditions is $N(0,t) = N_o$, which states that IMPs are inserted proximally into the membrane at a concentration that does not vary with time. At $t = 0$ the axon reduces

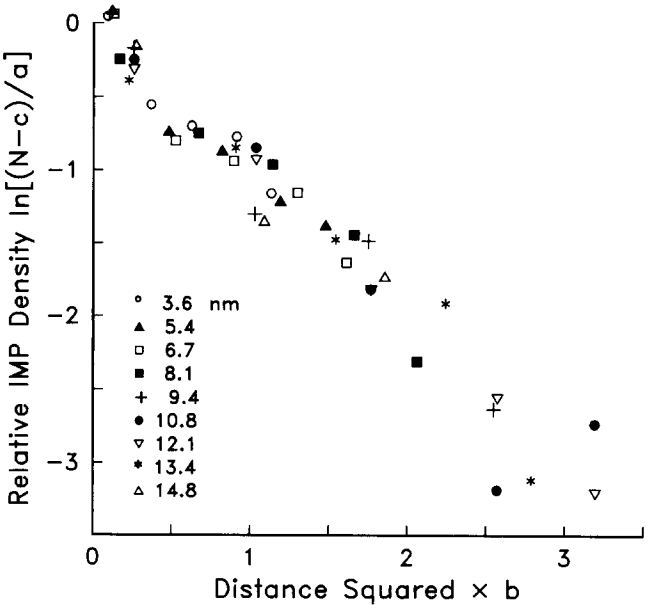

FIGURE 1 Distribution of plasmalemmal intramembrane particles (IMPs) along the growing axon (5 wk postoperative). The natural logarithm of the relative IMP density, normalized for particle size (cf. Eq. 1), has been plotted as a function of the squared distance. The data pool of 42 points (cf. reference 46) is represented in this figure. Note that a Gaussian function fits the entire population of data points, at least heuristically.

TABLE I

Gaussian Model: $y = a \exp(-bx^2) + c$

IMP Diameter	c* (=N_v)	a (=$N_o - N_v$)	D (=¼bt)	r^2	Sum of squares‡
(nm)	μm^{-2}	μm^{-2}	$cm^2/s \cdot 10^{-7}$		$\times 10^2$
3.6	74.0 ± 6.1	229.6	0.82	0.8970	37.17
5.4	31.6 ± 1.9	219.6	0.63	0.9068	30.10
6.7	35.1 ± 5.0	209.4	0.57	0.9108	28.00
8.1	14.1 ± 2.5	109.7	0.45	0.9375	22.59
9.4	14.1 ± 2.5	110.0	0.29	0.9471	19.03
10.8	0	67.8	0.29	0.8976	15.14
12.1	0	29.8	0.29	0.9964	15.12
13.4	0	13.5	0.33	0.9430	17.18
14.8	0	7.3	0.28	0.9272	23.90

Comparison of fit of Gaussian model to IMP density gradients of growing olfactory axons (5 wk postoperative).

* Density of IMPs in vesicles characteristic of growth cones.

‡ The sums of squares of relative differences is divided by five, the number of observations. The most distal 9.4-nm data point and the two most distal 14.8-nm data points were not included in the calculation because $N - N_v \leq 0$.

TABLE II

Moving-Boundary Diffusion Model: Least-squares Fit of the Unknown Parameters $N_o - N_v$ and τ; Estimates of N_o and D

IMP Diameter	$N_o - N_v$	N_o	τ (=tv²/D)	D	Relative sum of squares*
(nm)	μm^{-2}	μm^{-2}		$cm^2/s \cdot 10^{-7}$ (±%)	$\times 10^2$
3.6	298 ± 6.6	372.0	2.2 ± 0.1	1.75 ± 32%	1.13
5.4	295 ± 2.4	326.6	3.0 ± 0.1	1.29 ± 31%	1.52
6.7	290 ± 5.5	325.1	3.4 ± 0.1	1.13 ± 31%	1.83
8.1	140 ± 3.0	154.6	4.0 ± 0.1	0.96 ± 30%	3.37
9.4	134 ± 3.0	148.1	5.8 ± 0.1	0.66 ± 30%	30.99
10.8	93.6 ± 0.1	93.6	6.8 ± 0.1	0.57 ± 29%	8.27
12.1	43.5 ± 0.1	43.5	7.8 ± 0.1	0.49 ± 29%	0.61
13.4	18.4 ± 0.1	18.4	6.0 ± 0.1	0.64 ± 29%	4.68
14.8	10.3 ± 0.1	10.3	7.6 ± 0.1	0.51 ± 29%	40.14

Comparison of fit of moving-boundary diffusion model to IMP density gradients of growing olfactory axons (5 wk postoperative).

* The sums of squares of relative differences is divided by five, the number of observations.

to the origin; by continuity it follows that the initial value of N should also equal N_o. Thus, particle densities in newly emerging short axons are expected to approximate N_o (cf. below). A second boundary condition holds at the growth cone or, disregarding that growth cone's specialized domains, the distal axon area just behind it. Here, axolemmal IMP density is a function of particles contributed by diffusion from more proximal zones and by those inserted together with the membrane of the plasmalemmal precursor vesicles. Let N_v be the density of IMPs in these vesicles (cf. the term c in Eq. 1). It is assumed that N_v does not vary with time, i.e., that the insertion of IMPs into the growth cone and their appearance in the distal axon are independent of diffusion along the membrane. (The constancy of N_o and N_v, although not indispensable, is assumed in the absence of more detailed information.) Imagine now an observer rigidly attached to the distal end of the axon at $x = L(t)$. His reference frame moves at the velocity $V = dL/dt$ of the advancing growth cone with respect to the perikaryon. We assume that this velocity V is a constant. In this frame the observer would see a flux VN_v of particles contributed by the vesicles (inserted at the tip of the axon) and a flux $D\delta N/\delta x + VN$ due to diffusion and convection within the plasma membrane, in proximodistal direction. These fluxes must balance if IMPs are conserved in the axon periphery, and we thus obtain

$$D\frac{\delta N}{\delta x} + V(N - N_v) = 0, \text{ at } x = L(t). \quad [3]$$

This argument can be formalized with Green's theorem (9) applied to Eq. 2. The result, however, is nothing more than a statement of local mass conservation, under the proviso that the processes that deliver IMPs directly to the distal axon are decoupled from those within the membrane. The boundary condition in Eq. 3 is also known as the Stefan Condition (37). It holds even for variable V and N_v.

This diffusion problem does not appear to have an analytic solution. We must, therefore, resort to numerical methods. These are outlined in the Appendix. There it is shown that the problem can be expressed conveniently in dimensionless form through the following normalized variables: normalized concentration, $u = (N - N_v)/(N_o - N_v)$ [4]; fractional distance, $\xi = x/L = x/Vt$ [5]; and dimensionless time, $\tau = tV^2/D$ [6]. The form of τ is particularly interesting because, with the relation $L = Vt$, it shows the relative importance of convection (V) and diffusion (D/L) velocities. This ratio is also known as the Péclet Number (3). Large values of this number, as in our problem, indicate that the moving boundary outstrips the diffusion front, and one can expect steep diffusion profiles. On the other hand, small Péclet Numbers, often seen in metallurgical applications, show that a steady state is rapidly achieved.

The numerical solution is shown in Figs. 2 and 3. Fig. 2 illustrates that the density profiles are indeed linear for small values of the Péclet Number τ. In other words, for an initial, short period of time the IMP diffusion front can "track" the growth cone's motion, and approximate steady state is achieved. With increasing axon length, however, the steadily advancing growth cone begins to outstrip the IMPs's diffusion front. The region then appears effectively semiinfinite, density gradients become steep, and the total drop in density (at the axon tip, $x = L$) sharply increases with time. One then expects approximate Gaussian behavior. The transition between these states occurs in the range of values about $\tau = 1$. Fig. 3 illustrates in "Gaussian" form the data shown in Fig. 2. The abscissae of the two graphs are related through $x^2/4Dt = \xi^2\tau/4$. This figure shows that the solution approximately obeys Eq. 1 for large values of time, or more precisely, of τ. A least-

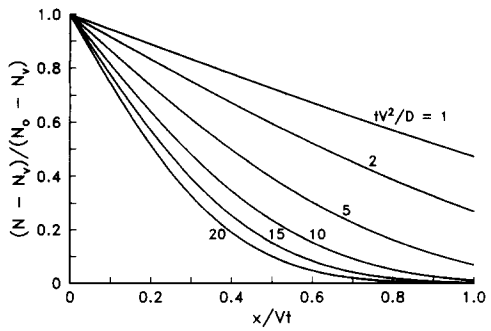

FIGURE 2 The normalized density, evaluated numerically from the diffusion model, is plotted linearly as a function of fractional distance. Each curve represents a record at the labeled value of dimensionless time.

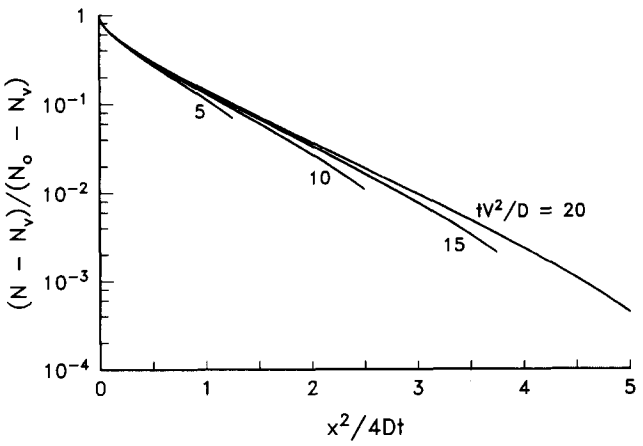

FIGURE 3 Same as Fig. 2, except that the numerical data are plotted logarithmically as a function of distance squared. Approximate Gaussian behavior is evident for large values of $\tau = tV^2/D$.

squares fit of the numerical data for $\tau = 20$ and values of $x^2/4Dt$ between 1 and 4 shows excellent correlation ($r^2 = 0.9987$) with a Gaussian tail, which has a characteristic exponent b given approximately by $(2.86\ Dt)^{-1}$ instead of the standard $(4\ Dt)^{-1}$. Note, however, the curvature in the profiles for small and large values of x, i.e., near the axon hillock and growth cone, respectively. This trend is, in fact, perceptible in the cumulative plot of densities shown in Fig. 1. These curved segments become relatively less significant as the axon grows longer. The proximal upward curvature results merely from plotting initial, linear segments of Fig. 2 as a function of x^2. The distal downward curvature is apparent only for $\tau > 1$. It is the effect of finite axon length ("size effect") on diffusion (cf. Eq. 3).

Data Fitting

The experimental data presented in the first paper of this series (46; Fig. 1) were obtained at fixed values of x, for a given growth time t (28 ± 5 d) and, thus, for a mean axon length of 9.66 ± 0.48 mm. As we observed before, N_v is measurable, so that the data $N - N_v$ (for each particle size) can be compared to the numerical solution of our diffusion model $(N_o - N_v) \times u(x/L, tV^2/D)$ at given values of x. This represents a two-parameter fit in the unknowns, namely $N_o - N_v$ and $\tau = tV^2/D$.

The numerical solution was first obtained for 100 values of tV^2/D evenly spaced in steps of $\Delta\tau = 0.2$, and for 50 values of x/L in equal steps of $\Delta\xi = 0.02$. As noted in the Appendix, we are then assured of an accuracy of at least three significant digits. The sum of the relative squared differences (divided by 5, the number of observations in each size class) was chosen as a measure of goodness of fit. (For rapidly decreasing functions, such as we have here, the sum of absolute squared differences biases the curve fit towards high-density values; fitting Eq. 1 by taking logarithms is equivalent to evaluating relative differences if these are small.) The sum of squares was evaluated for an array composed of all values of τ and a range of values of $N_o - N_v$. The minimum of the computed array then yielded the optimum values recorded in Table II. The uncertainty in $N_o - N_v$ is also recorded in Table II, and that in τ is estimated at ±0.1. Since $D = tV^2/\tau = L^2/t\tau$, one can then estimate D as well as its uncertainty δD:

$$\frac{\delta D}{D} = 2\frac{\delta L}{L} + \frac{\delta t}{t} + \frac{\delta \tau}{\tau}, \qquad [7]$$

$$= 2\frac{0.48}{9.66} + \frac{5}{28} + \frac{0.1}{\tau}.$$

The relative errors, due to the measurement of L, t, and τ are thus about 10%, 18%, and 1–4%, respectively. The measurement errors on axon length and growth time clearly dominate the total relative error on D (~30%). We also note in Tables I an II that the sum of squares for the moving-boundary model is considerably lower than the analogous measure for the Gaussian fit. However, one notices a relatively large sum of squares for the 9.4-nm class (cf. below). This also applies to the 14.8 nm IMPs, where total particle counts are low.

Fig. 4 shows the experimental data and the fitted curves from our model. The fits to our diffusion model appear good. However, it will be appreciated that data are available only for a single value of time. Thus, we have no way of verifying some of our assumptions, such as the time independence of V, N_o, and N_v. Data for a range of growth times should be satisfied by a single value of the diffusivity D for each IMP size class. Unfortunately, relevant data are not available at present.

We can, however, verify two other predictions of the moving-boundary diffusion model. When the axon reaches an appropriate target and growth stops, the IMP density gradient should relax and eventually change into a uniformly dense

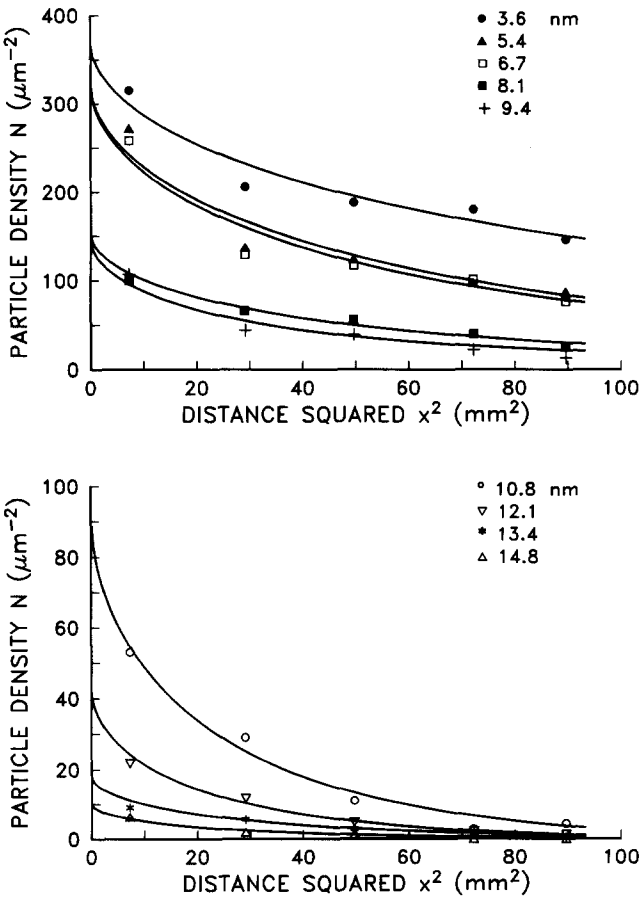

FIGURE 4 Density profiles (lines) fitted to experimental data (symbols) for IMPs with diameters of ≤9.4 nm (*top*) and with diameters of >9.4 nm (*bottom*). Note different scales for the particle densities.

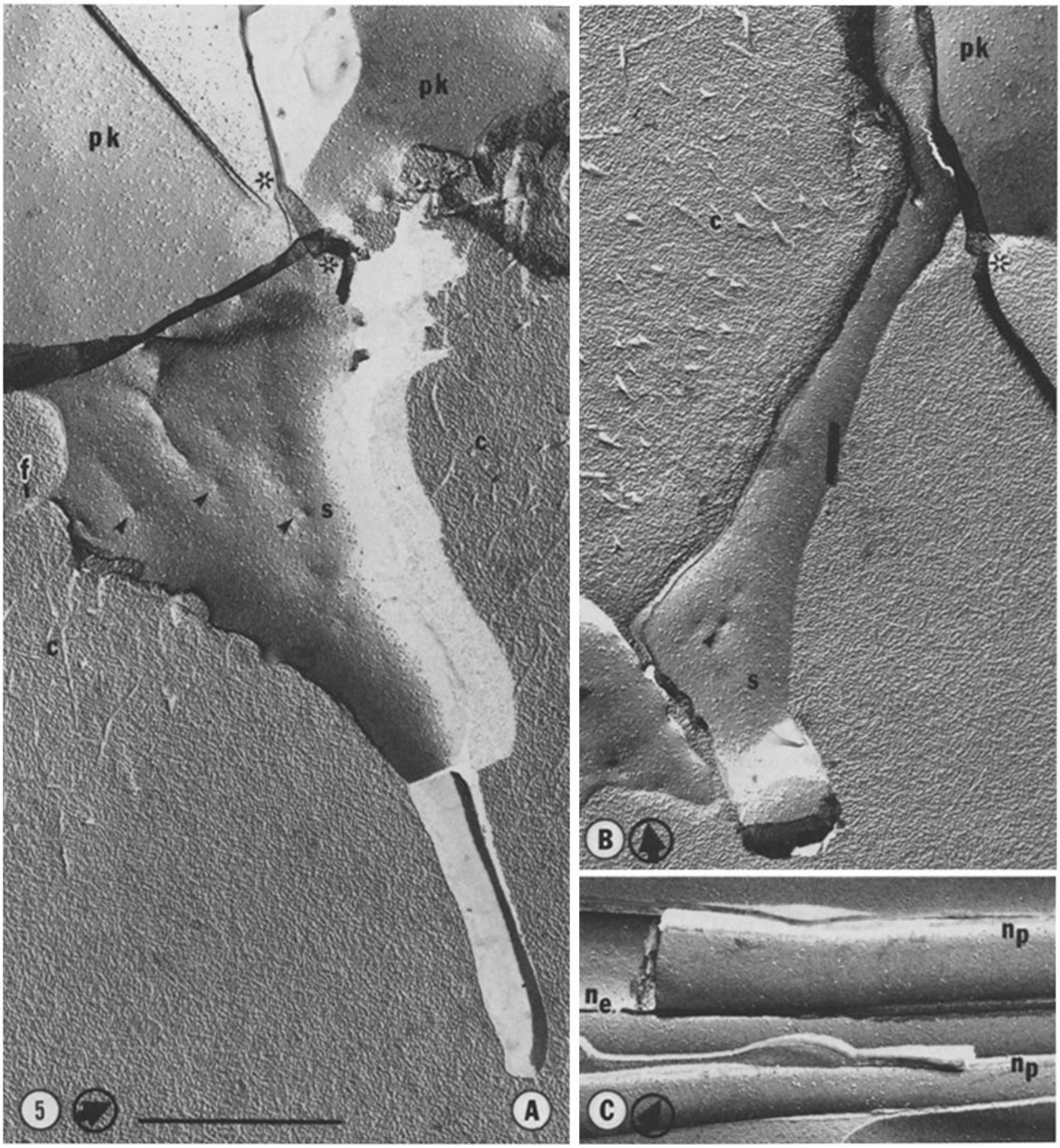

FIGURE 5 Electron micrographs of short neuritic sprouts as seen after freeze-fracture. (*A* and *B*) neurons dissociated from rat (newborn) superior cervical ganglia were plated on collagen-coated tissue culture dishes and freeze-fractured. Short sprouts (*s*; P-face) are seen to emerge from neuronal perikarya (*pk*). Note dimples (arrowheads) and small filopodia (*f*) characteristic of nerve growth cones (cf. companion paper, reference 46). However, plasmalemmal IMPs are present at high and apparently even density in the sprouts (~1,300/μm^2 for the area exposed in Fig. 5*B*). c, collagen fibers of culture substratum. Asterisks, folds in the replicas, probably caused by partial collapse of the bulging perikaryal region. (*C*) Distal region of a bundle of long neurites produced by an explant of rat superior cervical ganglion grown in vitro. These neurites were 1–2 mm long. Note low density of IMPs. n_P and n_e, P- and E-face neurites, respectively. Circled arrows, approximate shadowing directions. Bar 1 μm. ×33,000.

IMP profile. As already pointed out earlier (cf. 46), this is indeed the case. More significantly, our model predicts steady state distribution along the axon at early stages when values of $\tau \leq 1$. Steep density gradients should become apparent only for significantly larger values of τ. For olfactory axons, growing for 28 ± 5 d, τ ranges from 2.2 to 7.8 for the different IMP sizes (Table II). These values indicate that, for all IMP classes, axon length has already outstripped the diffusion front. To estimate particle distribution under the condition of a low Péclet Number, we examined emerging sprouts of dissociated neurons of rat superior cervical ganglia, grown in culture for 1 or 2 d. It is evident in Fig. 5, *A* and *B*, that very

short axons (here ~0.5 μm) display high densities and a near-equilibrium distribution of IMPs along their length. However, long shafts of neurites in this same system, grown for 5 to 7 d in vitro, display low IMP densities in distal regions (Fig. 5*C*; cf. 30)—as do growing olfactory axons. These observations indicate a transition in IMP profile from a steady state to a quasi-Gaussian gradient during neurite development, as predicted by our diffusion model.

Membrane Viscosity

As indicated in Table II, diffusion coefficients D can be calculated from the moving-boundary model and range from 0.51 to 1.75 × 10^{-7} cm^2/s for different IMP sizes. Thus, diffusivity is strikingly dependent upon IMP size. Assuming spherical shape of IMPs and diffusion conditions similar to those found in a macroscopic fluid phase, the diffusion coefficient D should be inversely proportional to the particle radius r according to the Stokes-Einstein Eq. 3:

$$D = \frac{k\,T}{6\pi r\eta}. \qquad [8]$$

In this equation, η = viscosity, k = Boltzmann's constant, T = absolute temperature. The calculated values of D have been plotted as a function of inverse particle diameter in Fig. 6. A linear relationship is evident as indicated by the regression line, $D = 8.7 \times 10^{-9}\ cm^2/s + (6.2 \times 10^{-14}\ cm^3/s)/2r$ (r^2 = 0.954), which passes through the ordinate just above the x/y intercept. Eq. 8 enables one to calculate membrane viscosity, η, which is proportional to $1/Dr$ and can be obtained from the slope of the regression line in Fig. 6. The membrane viscosity thus derived averages η = 7 centipoise. Our use of Eq. 8 with the Stokes expression for the drag on a particle involves the assumption of no slip at the surface. If there were slip, the numerical constant in the expression would change from 6π to 4π, and the calculated viscosity would be 50% greater (3). However, the assumption of no slip is more in keeping with the properties of solutions. In either case, the Stokes expression applies to diffusion of a spherical object in a solution and may not entirely satisfy the conditions of a quasicylindrical particle in a two-dimensional lipid bilayer.

Partition of Particles at the Axon Hillock

As already mentioned, the two extreme ends of the neuron, the perikaryon and the growth cone, are not part of the diffusion gradients formed by IMPs. Domains relatively rich in large IMPs are maintained in the growth cone (46). Furthermore, partition of IMPs between the perikaryon and the growing axon appears to occur at the axon hillock. As pointed out above, one can calculate the density of IMPs of specific size at the point of emergence of the growing axon (Table I). If these values, N_o, are divided by the measured densities of IMPs at the perikaryon, N_p, one obtains ratios of $N_o/N_p < 1$, which differ in mature and growing neurons. These partition coefficients are shown in Fig. 7. It is evident that, in the mature neuron (squares), IMP densities drop off sharply at the transition from the perikaryal to the axonal plasmalemma, and that the retention increases with particle size for IMPs with a diameter >8 nm. In the growing neuron (circles), however, partition of IMPs (except for the 8.1-nm class) at the axon hillock is much less pronounced and does not appear to be size-dependent >8.1 nm diameter. The result shows that perikaryal and axonal membrane domains in the growing neuron are not as sharply separated as in its mature counterpart, probably because of differences in the axon hillock region.

DISCUSSION

Diffusion Model of Particle Distribution in the Growing Axolemma

A priori, our freeze-fracture observations can be explained in various ways: (*a*) IMPs may be inserted into and anchored in the axolemma in specific locations so as to form the observed gradients. However, this would require separate vehicles or pathways of transport for each size class of IMPs. (*b*) The proteins forming IMPs may first diffuse within the axoplasm and then, after some time, enter the axolemma. However, most membrane proteins are incorporated into the lipid bilayer as they are synthesized (on the rough endoplasmic reticulum) and then shuttled to the cell surface (e.g., 38). Furthermore, large molecules and, especially, membranous elements, are actively transported at essentially constant velocity in the axoplasm (see, e.g., 15, 52). (*c*) Protein subunits of IMPs, possibly not visible by freeze-fracture electron microscopy, may be inserted into the axolemma as it is expanded and may then aggregate in proximodistal direction. However, this would not easily explain the actual shape of the gradients and is contradicted by the fact that we could not detect any increase in larger IMPs at the expense of smaller ones. (*d*) Intramembranous protein clusters may be released in large number into the extracellular space or internalized endocytotically at the growth cone, at a rate rapid enough to generate a downhill gradient in the axon shaft. However, no such evidence is available from freeze-fracture, tracer or other

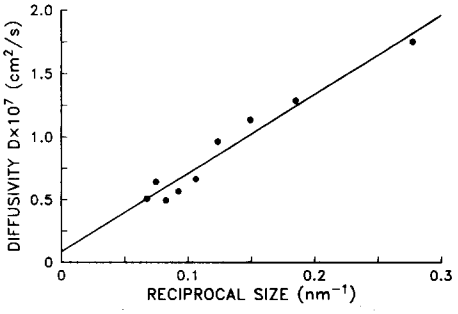

FIGURE 6 Measured diffusion coefficients as a function of inverse particle diameter. The Stokes-Einstein relation appears to be satisfied.

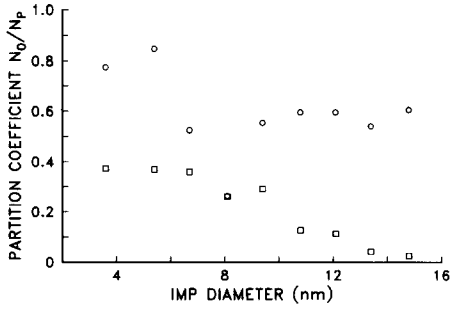

FIGURE 7 Partitioning of IMPs at axon hillock in growing and mature axons. Note increased retention of IMPs in the mature neuron. (○) Growing axon; (□) mature axon.

studies (30, 31, 46). (*e*) The simplest explanation of our findings is insertion of IMP proteins into the perikaryal plasmalemma followed by diffusion within this membrane into the axon (in a system that is continuously expanded by IMP-poor membrane at the advancing tip).

The mathematical analysis of our data supports this last view strongly: (*a*) the density profiles for each IMP size class fit exceptionally well the particle distributions calculated from our moving-boundary diffusion model (cf. Fig. 4); (*b*) the slopes of these gradients are dependent upon IMP size and proportional to $1/r$ as would be expected from a diffusion system; (*c*) two critical predictions of the diffusion model, high IMP densities in the axon periphery at the onset of growth and after the axon has reached its target, are borne out by our biological data. As explained earlier, some time is required for axon growth until axon length outstrips the IMP diffusion front. This is easily understood when considering that the time required for near-equilibration of IMP densities along the length of the advancing axon is very short at first but increases rapidly as a square function of total axon length. On the other hand, when an axon has reached its target and elongation has stopped, equilibration of IMP densities along the axon shaft produces a uniformly high density profile.

In summary, diffusion of IMPs into growing axolemma offers by far the best explanation of the freeze-fracture data. Most important, these results follow diffusion kinetics with a degree of precision that is likely to be causal rather than coincidental. Future biochemical studies will be aimed at corroborating, with independent experimental evidence, the adequacy of the diffusion model of membrane protein distribution in growing axons.

Biophysical Considerations

Before discussing the actual values of IMP diffusion coefficients, it is of interest to consider the striking influence of size on IMP diffusivity: between ~3.6 and 12 nm in diameter, D values change by a factor of 3.5. This finding is at variance with the predictions of the complex equations of Saffman and Delbrück (39), in which particle radius is of minor importance only.[1] IMP diffusivity is inversely proportional to diameter and, thus, obeys the classical equations of Fick and Stokes-Einstein. This is a surprising result because the Stokes-Einstein Equation (Eq. 8) was designed to relate the diffusion coefficient of a large sphere to the viscosity of an infinite, three-dimensional medium composed of very small particles. In contrast, the IMPs whose distribution we have studied range in diameter from 3.6 to 15 nm, while the membranes are two-dimensional sheets of 8–9 nm thickness. However, the laws governing diffusion in macroscopic systems have been found to apply to the diffusion of small molecules such as amino acids and sugars in aqueous solution (24) as well as ions, in the form of Walden's rule, which relates conductance and viscosity. The only limitation of these rules stems from the fact that the laws of physics are statistical in origin (43) and, thus, are valid only for the description of large numbers of particles or events. In our IMP distribution study, the condition of large numbers of events is fulfilled because of the long time of growth and diffusion and the large number of particles involved. Thus, the use of laws governing diffusion in macroscopic systems seems justified for the description of the membrane phenomena reported here.

A further issue pertinent to the size dependence of IMP diffusivity is IMP diameter itself. IMP diameter as determined electron microscopically in freeze-fracture replicas may be an overestimate because of the replica's thickness. However, this may be compensated, in part, by dehydration of the complexes due to "etching" (cf. companion paper, reference 46). Furthermore, it is not known whether a lipid coat contributes to the freeze-fracture image. Thus, our values for the actual diameter of the diffusing protein complexes are likely to suffer from a systematic error. This uncertainty is increased by the fact that it is not clear how IMP diameter relates to molecular weight and size. Irregularities are certain to exist, in those cases where only a small portion of a large protein is embedded in the membrane. One notable example is Na,K-ATPase, which has a molecular weight of about 280,000 and forms an unexpectedly small particle of ~9-nm diameter (e.g., 44, 50); a large portion of the protein appears to be exposed on the cytoplasmic side of the membrane. Furthermore, it is not clear how an IMP's diameter relates to its penetration depth through the membrane. While many protein complexes of different size may only partially reach through the membrane, larger IMPs are more likely to traverse it and, thus, to be exposed to both hydrophilic phases on either side. This may significantly influence the diffusion rates for such IMPs, depending upon the degree of anchoring and/or steric hindrance experienced outside the membrane (cf. 8, 39).

Lastly, IMPs—or the protein complexes they represent—are certainly not spheres but structures resembling cylinders, such as those discussed, e.g., by Saffman and Delbrück (39). In view of these open questions and potential irregularities regarding IMP size, the observed linear correlation between D and $1/r$ is actually surprising. It should be noted, however, that for IMPs >12-nm diameter, diffusivities no longer follow this rule closely, and that for most IMPs of ≥9.4-nm diameter (the diameter is greater than the membrane thickness) the fits of the diffusion curve (relative sums of squares, see Table II) are not as favorable as for the smaller IMPs.

Membrane viscosity has been calculated assuming (*a*) uniformity of the lipid bilayer throughout the growing axolemma and (*b*) knowledge of the actual size of the diffusing protein complexes. The resulting figures are low compared to other published values (cf. reference 14). Evidence obtained by others (11) as well as the change in mass fraction of protein along the axon (protein contained in IMPs; cf. below) indicate that the first assumption is a simplification. However, it is impossible at present to deal with this problem more accurately. The second issue, the uncertainty regarding IMP size and shape, has already been discussed. An IMP size overestimate would result in a decreased value for membrane viscosity. Furthermore, the Stokes-Einstein Equation (Eq. 8) seems to describe accurately the size-diffusivity relationship of IMPs but may not, in its present form, be adequate to calculate membrane viscosity.

[1] One of the reviewers kindly drew our attention to the paper by Vaz, W. L. C., M. Criado, V. M. C. Madeira, G. Schoellmann, and T. M. Jovin (1982, *Biochemistry*, 21:5608–5612) on the lateral mobility of three differently sized integral membrane proteins in synthetic bilayers. Within the small range of diffusant sizes tested (species of ~3, 3.4/4.6, and 6 nm diameter), these photobleach recovery studies show that the diffusion coefficient of the largest protein is reduced by 25 to 45% compared to those of the two smaller ones. Vaz et al. feel that this decrease of D is small and, thus, consistent with Saffman and Delbrück's hypothesis. However, the reduction in diffusivity they observed may not be significantly different from the one reported here (doubling of the size leads to a 50% reduction of D).

Neurobiological Considerations

The finding of IMP diffusion gradients in growing axons indicates that the axolemma is a significant pathway for the transfer of membrane components from the perikaryon into the axon periphery. This flux of membrane protein complexes is passive in nature and probably represents a minor fraction of proximodistally moving substances in the mature nerve. However, in the growing axon, especially near the perikaryon, the contribution of membrane components by lateral diffusion is substantial and likely to be qualitatively different from axoplasmically transported membrane constituents. It follows that for small values of τ, i.e., in short axon sprouts, growth cone membrane composition is different from that in longer axons with a steep IMP density gradient. This may suggest that an axon has to grow for some distance until its functional capacities are fully expressed. Such delayed growth cone capacitation would have important consequences for the formation of complex synaptic networks.

Diffusion of substances into the axolemma is greatly influenced by the nature of the axon hillock. Our analysis shows that the retention of IMPs in the perikaryal plasma membrane is relatively low in the growing nerve (albeit different for different IMP sizes), a condition that favors proximodistal flux. Retention increases with axon maturation, when perikaryon and axon become established as functionally different, separated cellular domains. Also segregated from the axolemma are parts of the plasma membrane of the nerve growth cone. Our findings suggest that these domains, which display considerably higher IMP densities than the distal axolemma, are maintained throughout axonal growth, apparently little influenced by the dynamics of the surrounding membrane regions. This stresses the concept of specialized functional membrane domains in the nerve growth cone.

Lateral Diffusion in a Chemical Gradient

Diffusion coefficients calculated from our measurements ($0.5–1.8 \cdot 10^{-7}$ cm^2/s) deserve some consideration. They are generally at least one order of magnitude greater than values calculated by others on the basis of photobleach recovery experiments in biological membranes (Table III; for review see, for example, references 8, 14). However, the discrepancy is considerably smaller when comparing our values with those observed in synthetic membranes (Table III; 7, 28, 51, 54) and those calculated on the basis of theoretical considerations for molecules in lipid monolayers and bilayers (4, 8, 28, 39). There are several important differences between our study and those executed by others (cf. Table III): (*a*) the time and distance observed, many days and millimeters in our case as opposed to seconds and micrometers in other studies; short observation times and distances, with few particles involved,

TABLE III

Diffusion Coefficients of Various Membrane Components

System	Membrane component	Diffusion coefficient ($cm^2 \cdot s^{-1}$)	°C	Method of determination‡	Reference
Lipids or lipid analogs					
Sciatic nerve		$5 \cdot 10^{-9}$	31	NMR	21
Neuroblastoma	* F-GM1§	$5–7 \cdot 10^{-9}$	—	FPR	11
Sarcoplasmic reticulum	* Lecithin	$2.5 \cdot 10^{-8}$	25	ESR	40
Liver microsomes	* Fatty acid	$1.1 \cdot 10^{-7}$	30	ESR	48
Lectin receptors‖					
Myoblasts	Con A receptor	$2.9 \cdot 10^{-11}$	23	FPR	41
Neurons	Con A receptor	$1.1–1.4 \cdot 10^{-10}$	22	FPR	55
Myoblasts	Con A receptor	$4–7 \cdot 10^{-10}$	22	E-F	36
Myoblasts	Con A receptor	$5.1 \cdot 10^{-9}$	22	E-F	35
Proteins					
Myotubes	Acetylcholine receptor	$4–5 \cdot 10^{-11}$	22	FPR	1
Neuroblastoma	RaE14 receptor¶	$1.8–3.5 \cdot 10^{-10}$	—	FPR	11
Mast cells	Fc receptor	$2 \cdot 10^{-10}$	—	FPR	42
Pheochromocytoma	Nerve growth factor receptor	$8 \cdot 10^{-10}$	RT**	FPR	22
Inner mitochondrial membrane	Miscellaneous proteins	$8.3 \cdot 10^{-10}$	20	E-FF	47
Myotubes	Miscellaneous antigens	$1–3 \cdot 10^{-9}$	RT	PS	13
Myoblasts	Acetylcholine receptor	$2.6 \cdot 10^{-9}$	22	RS	33
Retinal rod outer segment	Rhodopsin	$3–5 \cdot 10^{-9}$	20	PR	23, 34
Components in synthetic membranes					
Lipid multibilayer	RBC glycophorin, band 3‡‡	$\sim 1.7 \cdot 10^{-8}$	24	FPR	7, 54
Planar lipid bilayer	Synthetic glycolipid	$3 \cdot 10^{-8}$		FPR	53
Lipid multibilayer	Gramicidin C	$4 \cdot 10^{-8}$	30	FPR	51

* Asterisk indicates labeled derivative.

‡ E-F, Relaxation after redistribution by electrophoresis in situ; marker, fluorescent ligand. E-FF, Relaxation after redistribution by electrophoresis in situ; distribution analysis of components by freeze-fracture. ESR, Electron spin resonance. FPR, Fluorescence photobleach recovery. PR, Photobleach recovery (no extrinsic probe). PS, Patch spreading after labeling with fluorescent probe. RS, Recovery of acetylcholine sensitivity after toxin labeling.

§ Fluorescein-labeled analog of ganglioside GM_1.

‖ Mixed population of glycoproteins. *Con A*, concanavalin A.

¶ Surface antigen that cross-reacts with an antibody generated to mouse E14 lymphoid cells.

** *RT*, room temperature.

‡‡ Erythrocyte membrane proteins.

may result in greater experimental error, and the results for small numbers of events may not equal those for large numbers of events (cf. above). (*b*) The absence of "invasive" experimental manipulations, such as surface labeling and irradiation with intense light, which have been used in many other studies (cf. reference 18). (*c*) Most other membrane systems investigated contain a relatively high mass fraction of protein. In macroscopic systems, increased volume fraction, Φ, of spherical particles in solution would be expected to increase the apparent viscosity as follows:

$$\eta = \eta_o(1 + 2.5\Phi). \qquad [9]$$

Relative to the middle segment of the growing axon, where the protein mass fraction is negligibly small ($\Phi = 0.017$), one would expect the diffusion rate of IMPs to be slowed down by a factor of 0.63 in, for example, the disk membrane of the retinal rod outer segment of the frog, solely because of its larger protein mass fraction (28).[2] (*d*) Furthermore, the lipid composition and the degree of cytoplasmic anchoring of membrane proteins may differ greatly in the various experimental systems studied (cf. 7). Anchoring may be particularly weak in the developing, growing axons described here. (*e*) The last—and probably most significant—difference is that the systems studied previously (except reference 47, for very short time periods) are isoconcentration systems in which tracer diffusivity is analyzed, whereas in growing axolemma the diffusing species form chemical gradients.

The difference between chemical and tracer diffusivities is well known in metallurgy, where it has been described by Darken's Relation (10). Analogous explanations can be found in biology, in the field of nonequilibrium thermodynamics. Nonequilibrium processes depend upon the rate of (irreversible) production of entropy as formulated by Onsager, Katchalsky, and others (e.g., 19, 26, 27). This dissipation of free energy (obviously not occurring in isoconcentration systems) is, in fact, the major driving force of diffusion in a chemical gradient. In the growing neuron this nonequilibrium process is maintained for long time periods by continued axon elongation. Therefore, the diffusion measurements presented here are not readily comparable to those described before (cf. Table III). Rather, they form a complementary set of observations indicating that, under certain circumstances, IMPs or membrane protein complexes can laterally diffuse at far more rapid rates than previously assumed.

APPENDIX

There exist a wide variety of numerical methods for the solution of Stefan Problems. We have applied two of these; both are efficient finite difference algorithms that yield equivalent results. The first method is due to Douglas and Gallie (12), who showed how one can choose variable time steps such that one always tracks the boundary's motion in the (x,t) plane. This method has been extended (17) to include the effect of mixed boundary conditions such as we have, cf. Eq. 3. Our problem, however, is simpler than most because the velocity V of the growth cone is known and is assumed constant. The following method, due to Landau (20), is then strongly recommended.

[2] On the basis of the IMP data of Besharse and Pfenninger (2) and assuming spherical particles embedded in a membrane of 9 nm thickness, one can calculate a protein mass fraction in the lipid bilayer of $\Phi = 0.262$.

The key to this second method is a simple change of the space variable that immobilizes the boundary, cf. Eq. 5. This substitution also has intuitive appeal since distances are now measured in fractions of the axon length at time t. The physical meaning of the time-like variable τ has been discussed earlier. In the variables, Eqs. 4–6, it is easy to recast our problem, Eqs. 2 and 3 and subsidiary conditions, in the form:

$$\tau^2\frac{\delta u}{\delta \tau} = \frac{\delta^2 u}{\delta \xi^2} + \xi\tau\frac{\delta u}{\delta \xi}, \text{ for } 0<\xi<1,\ \tau>0, \qquad [A.1]$$

$u = 1$ on the boundaries $\xi = 0$ and $\tau = 0$, and the Stefan Condition

$$\frac{\delta u}{\delta \xi} + \tau u = 0, \text{ for } \xi = 1,\ \tau>0. \qquad [A.2]$$

Equation A.1 is a parabolic partial differential equation with variable, but known, coefficients. It can easily be solved by a variety of standard finite difference schemes. We have found that the fully implicit scheme with centered space differences (6) gave excellent results. As noted in the text, the space and time meshes were chosen to assure us of at least three significant digits.

The authors wish to express their gratitude to Linda B. Friedman and Kathleen Silberman for skillful assistance with the completion of this manuscript.

This work was supported by National Institutes of Health (NIH) grant NS 13466 to K. H. Pfenninger, a fellowship to R. Small from the N.Y. State Health Research Council, and grants HL 15932 from the NIH and N00014-83-K-0043 from the ONR to M. Blank. R. Small also was a Jordan Fellow of the National Spinal Cord Injury Foundation.

Received for publication 21 September 1982, and in revised form 30 September 1983.

REFERENCES

1. Axelrod, D., P. Ravdin, D. E. Koppel, J. Schlessinger, W. W. Webb, E. L. Elson, and T. R. Podleski. 1976. Lateral motion of fluorescently labeled acetylcholine receptors in membranes of developing muscle fibers. *Proc. Natl. Acad. Sci. USA.* 73:4594–4598.
2. Besharse, J. C., and K. H. Pfenninger. 1980. Membrane assembly in retinal photoreceptors. I. Freeze-fracture analysis of cytoplasmic vesicles in relationship to disc assembly. *J. Cell Biol.* 87:451–463.
3. Bird, R. B., W. E. Stewart, and E. N. Lightfoot. 1960. Transport Phenomena. John Wiley & Sons, New York.
4. Blank, M., and J. S. Britten. 1965. Transport properties of condensed monolayers. *J. Colloid Sci.* 20:789–800.
5. Bretscher, M. S. 1973. Membrane structure: some general principles. *Science (Wash. DC).* 181:622–629.
6. Carnahan, B., H. A. Luther, and J. O. Wilkes. 1969. Applied Numerical Methods. John Wiley & Sons, New York.
7. Chang, C.-H., H. Takeuchi, T. Ito, K. Machida, and S.-I. Ohnishi. 1981. Lateral mobility of erythrocyte membrane proteins studied by the fluorescence photobleaching recovery technique. *J. Biochem.* 90:997–1004.
8. Cherry, R. J. 1979. Rotational and lateral diffusion of membrane proteins. *Biochim. Biophys. Acta* 559:289–327.
9. Courant, R., and D. Hilbert. 1953. Methods of Mathematical Physics. Vol. I. Interscience Publishers, New York.
10. Darken, L. S. 1948. Diffusion, mobility and their interrelation through free energy in binary metallic systems. *Transactions of the American Institute of Metallurgical Engineers.* 175:184–201.
11. de Laat, S. W., P. T. Van der Saag, and E. L. Elson. 1979. Lateral diffusion of membrane lipids and proteins is increased specifically in neurites of differentiating neuroblastoma cells. *Biochim. Biophys. Acta.* 558:247–250.
12. Douglas, J., Jr., and T. M. Gallie, Jr. 1955. On the numerical integration of a parabolic differential equation subject to a moving boundary condition. *Duke Mathematics Journal.* 22:557–571.
13. Edidin, M., and D. Fambrough. 1973. Fluidity of the surface of cultured muscle fibers: rapid lateral diffusion of marked surface antigens. *J. Cell Biol.* 57:27–37.
14. Edidin, M. 1974. Rotational and translational diffusion in membranes. *Annu. Rev. Biophys. Bioeng.* 3:179–201.
15. Grafstein, B., and D. S. Forman. 1980. Intracellular traffic in neurons. *Physiol. Rev.* 60:1167–1283.
16. Graziadei, P. P. C., and R. S. deHan. 1973. Neuronal regeneration in frog olfactory

system. *J. Cell Biol.* 59:525–530.
17. Gupta, R. S., and Kumar, D. 1981. Variable time step methods for one-dimensional Stefan Problems with mixed boundary condition. *International Journal of Heat and Mass Transfer.* 24:251–259.
18. Jacobson, K., E. Elson, D. Koppel, and W. Webb. 1982. Fluorescence photobleaching in cell biology *Nature* (*Lond.*). 295:283–284.
19. Katchalsky, A. 1967. Membrane thermodynamics. *In* The Neurosciences: A Study Program. G. C. Quarton, T. Melnechuk, and F. O. Schmitt, editors. The Rockefeller University Press, New York.
20. Landau, H. G. 1950. Heat conduction in a melting solid. *Quarterly of Applied Mathematics.* 8:81–94.
21. Lee, A. G., N. J. M. Birdsall, and J. C. Metcalfe. 1973. Measurement of fast lateral diffusion of lipids in vesicles and in biological membranes by ^1H nuclear magnetic resonance. *Biochemistry.* 12:1650–1659.
22. Levi, A., Y. Schechter, E. J. Neufeld, and J. Schlessinger. 1980. Mobility, clustering, and transport of nerve growth factor in embryonal sensory cells and in a sympathetic neuronal cell line. *Proc. Natl. Acad. Sci. USA.* 77:3469–3473.
23. Liebman, P. A., and G. Entine. 1974. Lateral diffusion of visual pigment in photoreceptor disk membranes. *Science* (*Wash. DC*). 185:457–459.
24. Longsworth, L. G. 1953. Diffusion measurements, at 25°, of aqueous solutions of amino acids, peptides and sugars. *J. Am. Chem. Soc.* 75:5705–5709.
25. McNutt, M. S. 1977. Freeze-fracture techniques and application to the structural.analysis of the mammalian plasma membrane. *Cell Surf. Rev.* 3:95–126.
26. Onsager, L. 1931. Reciprocal relations in irreversible processes. I. *Physiol. Rev.* 37:405–426.
27. Onsager, L. 1931. Reciprocal relations in irreversible processes. II. *Physiol. Rev.* 38:2265–2279.
28. Peters, R., and R. J. Cherry. 1982. Lateral and rotational diffusion of bacterio-rhodopsin in lipid bilayers: experimental test of the Saffman-Delbruck equations. *Proc. Natl. Acad. Sci. USA.* 79:4317–4321.
29. Pfenninger, K. H. 1982. Axonal transport in the sprouting neuron: transfer of newly synthesized membrane components to the cell surface. *In* Axoplasmic Transport in Physiology and Pathology. Weiss, D. G. and A. Gorio, editors. Springer-Verlag, Berlin. pp. 52–61.
30. Pfenninger, K. H., and R. P. Bunge. 1974. Freeze-fracturing of nerve growth cones and young fibers: a study of developing plasma membrane. *J. Cell Biol.* 63:180–196.
31. Pfenninger, K. H., and M. F. Maylié-Pfenninger. 1981. Lectin labeling of sprouting neurons. II. Relative movement and appearance of glycoconjugates during plasmalemmal expansion. *J. Cell Biol.* 89:547–559.
32. Pfenninger, K. H., and E. R. Rinderer. 1975. Methods for the freeze-fracturing of nerve tissue cultures and cell monolayers. *J. Cell Biol.* 65:15–28.
33. Poo, M. 1982. Rapid lateral diffusion of functional ACh receptors in embryonic muscle cell membrane. *Nature* (*Lond.*). 295:332–334.
34. Poo, M., and R. A. Cone. 1974. Lateral diffusion of rhodopsin in the photoreceptor membrane. *Nature* (*Lond.*). 247:438–440.
35. Poo, M., J. W. Lam, N. Oida, and A. W. Chao. 1979. Electrophoresis and diffusion in the plane of the cell membrane. *Biophys. J.* 26:1–22.
36. Poo, M., W. Poo, and J. W. Lam. 1978. Lateral electrophoresis and diffusion of concanavalin A receptors in the membrane of embryonic muscle cell. *J. Cell Biol.* 76:483–501.
37. Rubinstein, L. I. 1967. The Stefan Problem. Translations of Mathematical Monographs. American Mathematical Society, Providence, Rhode Island. Vol. 27.
38. Sabatini, D., G. Kreibich, T. Morimoto, and M. Adesnik. 1982. Mechanisms for the incorporation of proteins in membranes and organelles. *J. Cell Biol.* 92:1–22.
39. Saffman, P. G., and M. Delbrück. 1975. Brownian motion in biological membranes. *Proc. Natl. Acad. Sci. USA.* 72:3111–3113.
40. Scandella, C. J., P. Devaux, and H. M. McConnell. 1972. Rapid lateral diffusion of phospholipids in rabbit sarcoplasmic reticulum. *Proc. Natl. Acad. Sci. USA.* 69:2056–60.
41. Schlessinger, J., D. E. Koppel, D. Axelrod, K. Jacobson, W. W. Webb, and E. L. Elson. 1976. Lateral transport on cell membranes. Mobility of concanavalin A receptors on myoblasts. *Proc. Natl. Acad. Sci. USA.* 73:2409–2413.
42. Schlessinger, J., W. W. Webb, E. L. Elson, and H. Metzger. 1976. Lateral motion and valence of Fc receptors on rat peritoneal mast cells. *Nature* (*Lond.*). 264:550–552.
43. Schrödinger, E. 1944. What Is Life? Cambridge University Press, Cambridge.
44. Skriver, E., A. B. Maunsbach, and P. L. Jorgensen. 1980. Ultrastructure of Na, K-transport vesicles reconstituted with purified renal Na, K-ATPase. *J. Cell Biol.* 86:746–754.
45. Singer, S. J., and G. L. Nicolson. 1972. The fluid mosaic model of the structure of cell membranes. *Science* (*Wash. DC*). 175:720–731.
46. Small, R., and K. H. Pfenninger. 1984. Components of the plasma membrane of growing axons. I. Distribution of intramembrane particles. 98:1422–1433.
47. Sowers, A. E., and C. R. Hackenbrock. 1981. Rate of lateral diffusion of intramembrane particles: measurement by electrophoretic displacement and rerandomization. *Proc. Natl. Acad. Sci. USA.* 78:6246–6250.
48. Stier, A., and E. Sackmann. 1973. Spin labels as enzyme substrates. Heterogeneous lipid distribution in liver microsomal membranes. *Biochim. Biophys. Acta.* 311:400–408.
49. Strichartz, G. R., R. K. Small, and K. H. Pfenninger. 1984. Components of the plasma membrane of growing axons. III. Saxitonin binding to sodium channels. 98:1444–1452.
50. Sweadner, K. J., and S. M. Goldin. 1980. Active transport of sodium and potassium ions. *N. Engl. J. Med.* 302:777–783.
51. Tank, D. W., E. S. Wu, P. Meers, and W. W. Webb. 1981. Lateral diffusion of gramicidin C in phospholipid multibilayers containing 0–50 mole% cholesterol. *Biophys. J.* 33:109*a*. (Abstr.)
52. Weiss, D. G., editor. 1982. Axoplasmic Transport in Physiology and Pathology. Springer Verlag, Berlin.
53. Wolf, D. E., J. Schlessinger, E. L. Elson, W. W. Webb, R. Blumenthal, and P. Henkart. 1977. Diffusion and patching of macromolecules on planar lipid bilayer membranes. *Biochemistry.* 16:3476–3483.
54. Wu, E. S., P. S. Low, and W. W. Webb. 1981. Lateral diffusion of glycophorin reconstituted into phospholipid multibilayers. *Biophys. J.* 33:109*a*. (Abstr.)
55. Zagyansky, Y., P. Benda, and J. C. Bisconte. 1977. Restricted lateral diffusion of concanavalin A receptors of different malignant cells of the nervous system. *FEBS* (*Fed. Eur. Biochem. Soc.*) *Lett.* 77:206–208.